

Composite Generalized Dynamic Predictive Control with Self-Tuning Horizon for Wide-Range Speed Regulation of PMSM Drives

Zhongkun Cao, Jianliang Mao, *Member, IEEE*, Xin Dong, Rafal Madonski, *Senior Member, IEEE*, Chuanlin Zhang, *Senior Member, IEEE*, and Jun Yang, *Fellow, IEEE*

Abstract—This article proposes and investigates a novel composite generalized dynamic predictive control (GDPC) approach for wide-range speed regulation of permanent magnet synchronous motor (PMSM) drives under a non-cascade configuration. Firstly, to eliminate negative effects arising from both matched and mismatched disturbances within the receding-horizon optimization of the baseline generalized predictive control (GPC) design, two high-order sliding mode observers (HOS-MOs) are constructed for disturbance estimation, which allows for offset-free tracking of the reference speed. Furthermore, a novel self-tuning horizon mechanism is introduced for wide-range speed regulation scenarios of PMSM drives. This feature enables autonomous and dynamic adjustment of the prediction horizon across diverse speed regulation ranges, resulting in significantly improved performance optimization compared to the conventional GPC method. Finally, the proposed GDPC methodology is implemented on a digital signal processor (DSP) hardware system. The simulations and experiments demonstrate the effectiveness of the proposed control approach.

Index Terms—generalized predictive control, PMSM speed regulation, disturbance rejection, self-tuning horizon.

I. INTRODUCTION

PERMANENT magnet synchronous motors (PMSM) have been widely used in electric vehicles, robots, servo systems, and aerospace applications due to their simple design, high energy density and efficiency [1]–[3]. However, due to the strong coupling and multi-source disturbances of PMSM drives, there still remains a great challenge in achieving high-speed control accuracy and fast dynamic performance. For example, in most applications, such as electric vehicles [4] and spindle drives [5], require a wide range of speed regulation under time-varying disturbances, which puts more stringent demands on the high-performance of PMSM drives.

It is well known that field-oriented control (FOC) with a cascade structure is widely used in PMSM drives owing to its

This work was supported in part by the National Natural Science Foundation of China under Grant 62173221 and Grant 62203292, in part by the Ministry of Education Chunhui Plan Cooperative Research Projects under Grant 202200890, and in part by the U.K. Engineering and Physical Science Research Council (EPSRC) New Investigator Award under Grant EP/W027283/1 (*Corresponding author: Jianliang Mao*)

Zhongkun Cao, Jianliang Mao, Xin Dong, and Chuanlin Zhang are with the College of Automation Engineering, Shanghai University of Electric Power, Shanghai 200090, China (e-mail: caozhongkun@mail.shiep.edu.cn; jl_mao@shiep.edu.cn; xxddong@shiep.edu.cn; clzhang@shiep.edu.cn).

Rafal Madonski is with the Faculty of Automatic Control, Electronics and Computer Science, Silesian University of Technology, Gliwice 44-100, Poland (r.madonski@polsl.pl).

Jun Yang is with the Department of Aeronautical and Automotive Engineering, Loughborough University, Loughborough LE11 3TU, UK (e-mail: j.yang3@lboro.ac.uk).

favorable steady-state performance and low torque chattering [6]. Typically, conventional FOC configurations for speed regulation of PMSM drives necessitate meticulous design and tuning of three PI controllers [7]. However, the transient-time response capability is substantially limited in such case to avoid undesired control overshoot, which restricts the enhancement of dynamic performance [7]. Fortunately, thanks to the rapid development of advanced control theory, several elegant control approaches have been proposed, such as sliding mode control (SMC) [8], [9], adaptive control [10], [11], disturbance rejection control [12]–[14], and model predictive control (MPC) [15]–[19], etc.

As an optimal control approach, MPC has gained increasing attention among control practitioners due to its distinct advantages of optimizing dynamic performance and handling constrained problems [20], and thus has been widely applied in PMSM drives for improved performance. Specifically, in [16]–[18], the cascade MPC approach is proposed, in which the PI controller for the speed loop or current loop in the cascade structure is replaced by MPC to enhance the control performance of the PMSM system. However, since the cascade configuration of speed and current controllers, the dynamic response performance of speed regulation is still limited to a certain extent [21]. To achieve high control dynamics in speed, a direct predictive speed control approach is investigated in [22]–[24], which yields the desired q -axis voltage directly via a single active speed controller. However, the adoption of the non-cascade structure necessitates a higher order system model, resulting in a complex control algorithm [25]. The substantial computational burden of solving an optimal problem at each control iteration poses a significant challenge to the practical implementation of these approaches. Moreover, due to the removal of the current loop, mismatched disturbance and uncertainties inevitably pose a significant challenge to alleviating performance degradation [26]. Therefore, the compensation of matched/mismatched disturbance emerges as a pivotal factor in optimizing the control performance of MPCs.

By analyzing the above references, it is notable that the aforementioned MPCs are mainly based on a discrete-time model, in which the optimization effect primarily depends on the value of the sampling period. As a preferred solution to this issue, a generalized predictive control (GPC) approach is proposed in [27]. This approach is based on a continuous-time system model and offline receding-horizon optimization via Taylor expansion approximation to minimize the cost function. Compared to the MPC methods based on a discrete-time

model, the demand for a real-time solution to optimization problem is neatly avoided, resulting in a slight computational burden and intuitive parameter adjustment. In addition, it is also worth noting that the aforementioned predictive control approaches are generally implemented by configuring a fixed value for the prediction horizon, which usually requires engineers to select by trial and error. Although this conservative treatment can result in satisfactory control performance for PMSM drives under fixed or slowly changing operating conditions, issues with performance optimization deviation may be encountered when considering significantly varied operating conditions, such as wide range speed regulation or sudden external load changes [28]. To overcome this limitation, an adaptive receding horizon-based predictive control strategy is proposed in [29], [30], which allows for online adjustment of the horizon based on different operating conditions, thereby enhancing system adaptability. However, direct compensation of time-varying mismatched disturbances is not explicitly considered in these methods.

Motivated by the preceding discussion, this article proposes a novel composite generalized dynamic predictive control (GDPC) approach, driven by the following main objectives: i) Achieve accurate tracking of the given reference signals in the presence of disturbances while exhibiting satisfactory robustness against disturbances; ii) Enhance the performance optimization capability of the PMSM system across a wide-range speed regulation scenarios. Towards this end, firstly, a hierarchical compensation strategy by HOSMOs for both matched and mismatched disturbances, with the concurrent consideration of time-varying mismatched disturbances, is enabled by utilizing the disturbance/uncertainty estimation and attenuation (DUEA) technique. Subsequently, an offset-free predictive speed controller based on prediction accuracy enhancement is achieved by incorporating disturbance estimation into the baseline GPC design process. Finally, a novel self-tuning horizon mechanism is developed through a concise dynamical function correlated with the speed-tracking error. This method empowers the system to dynamically adjust the prediction horizon according to varying working conditions, achieving autonomous and real-time adjustment of the performance optimization effects for the system. Compared to the established state of the art in this area, the main contributions and novelties of this paper are listed as follows.

- 1) By fusing the merits of the DUEA technique and MPC approaches, a continuous-time offset-free composite predictive speed controller with a non-cascade structure is developed, which achieves the prominent disturbance rejection performance while neatly circumventing the online optimization problem in existing MPCs, resulting in a significant reduction in computational effort.
- 2) Instead of selecting a fixed prediction horizon value from engineering experience, the proposed GDPC method exploits a concise self-tuning mechanism for prediction horizon selection, which actively provides PMSM drives with a performance self-optimization capability under wide-range speed regulation.

The remainder of this article is organized as follows. The

pre-treatment of the PMSM system is shown in Section II. Section III mainly presents the detailed design process of the proposed GDPC approach. The simulation tests are presented in Section IV. Section V provides the extension of the basic control requirements. Comparative experiments with different cases are presented in Section VI. Section VII summarizes the paper. Finally, the rigorous stability analysis of the closed-loop system is provided in the Appendix.

II. PROBLEM FORMULATION

This section presents the considered dynamic model of the PMSM speed regulation system. Next, utilizing the obtained state-space model, ideal reference values for system states are analyzed. Then, the equivalent system error dynamics is built.

A. Dynamics Model of PMSM

The mathematical model of a surface-mounted PMSM (SPMSM) in the d - q coordinates frame can be defined as [26]

$$\begin{cases} \dot{\omega} = \frac{1}{J} \left(\frac{3}{2} n_q \psi_f i_q - B_m \omega - T_L \right), \\ \dot{i}_d = \frac{1}{L_s} (-R_s i_d + n_q \omega L_s i_q + u_d), \\ \dot{i}_q = \frac{1}{L_s} (-R_s i_q - n_p \omega L_s i_d - n_q \psi_f \omega + u_q), \end{cases} \quad (1)$$

where ω is the mechanical angular velocity, J is the rotor inertia, n_q is the number of pole pairs, ψ_f is the rotor flux linkage, B_m is the viscous frictional coefficient, T_L is the load torque, R_s is the stator resistance, L_s is the stator inductance, i_d , i_q , u_d , and u_q are the stator currents and voltages of the d -axis and q -axis, respectively.

In general, the FOC strategy is usually employed for the considered SPMSM, in which the d -axis current reference, denoted as i_d^* , is set as zero to achieve the maximum torque-to-current ratio. Therefore, this makes it possible to control the torque and speed of the motor without affecting the magnetic field orientation. On account of this fact, this paper mainly focuses on the non-cascade design of the speed and q -axis current controllers.

By defining $x_1 = \omega_{\text{ref}} - \omega$, $x_2 = \frac{B_m}{J} \omega_{\text{ref}} - \frac{3n_p \psi_f}{2J} i_q$ as the oriented-control system state variables, where ω_{ref} is the reference speed, the subsystem for the speed and q -axis current controllers can be separated from system (1) resulting in

$$\begin{cases} \dot{x}_1 = x_2 + f_1(\bar{x}) + d_1, \\ \dot{x}_2 = u_1 + f_2(\bar{x}) + C_1 + d_2, \\ y_1 = x_1, \end{cases} \quad (2)$$

where $\bar{x} = (x_1, x_2)^\top$ is the system state vector, $u_1 = -\frac{3n_p \psi_f}{2J L_s} u_q$ and y_1 are the input and output of the system, respectively, d_1 represents the lumped mismatched disturbance, primarily composed of external load $\frac{T_L}{J}$, and d_2 is regarded as the matched disturbances including internal uncertainties and unmodeled dynamics, with

$$\begin{aligned} f_1(\bar{x}) &= -\frac{B_m}{J} x_1, \quad C_1 = \frac{1}{J L_s} (R_s B_m + \frac{3}{2} n_p^2 \psi_f^2) \omega_{\text{ref}}, \\ f_2(\bar{x}) &= -\frac{3n_p^2 \psi_f^2}{2J L_s} x_1 - \frac{R_s}{L_s} x_2 + \frac{3n_p^2 \psi_f}{2J} (\omega_{\text{ref}} - x_1) i_d. \end{aligned}$$

Assumption 1: The matched and mismatched disturbances in system (2) satisfy the condition that $\sup\{|d_1|, |\dot{d}_1|, |d_2|\} \leq D$, where D is a positive constant.

B. Control Objective

Aiming at achieving offset-free speed tracking for PMSM drives with time-varying disturbances, a set of steady-state reference signals with disturbance compensation is introduced. Then, assuming that the disturbances are exactly well known, the ideal steady-state reference signals can be naturally constructed from system (2) as follows

$$\begin{cases} x_1^* = 0, x_2^* = -d_1, \\ u_1^* = \dot{x}_2^* - f_2(\bar{\mathbf{x}}^*) - C_1 - d_2, \end{cases} \quad (3)$$

where $\bar{\mathbf{x}}^* = (x_1^*, x_2^*)^\top$, x_1^* , x_2^* and u_1^* are the reference steady-state values of x_1 , x_2 and u_1 , respectively.

Furthermore, by defining $\delta_\omega = x_1 - x_1^*$, $\delta_q = x_2 - x_2^*$, and $v_q = u_1 - u_1^*$ as the ideal system state errors, the equivalent system error dynamics can be expressed as

$$\begin{cases} \dot{\delta}_\omega = \delta_q + f_1(\bar{\mathbf{x}}) - f_1(\bar{\mathbf{x}}^*), \\ \dot{\delta}_q = v_q + f_2(\bar{\mathbf{x}}) - f_2(\bar{\mathbf{x}}^*). \end{cases} \quad (4)$$

At this point, the control objective of this paper is to design a composite controller v_q , such that δ_ω and δ_q quickly converge to zero even in the presence of widely varying operating conditions.

III. CONTROLLER DESIGN UNDER FOC STRUCTURE

In this section, the design structure of the proposed composite GDPC methodology is presented step-by-step.

A. Disturbance Reconstruction

Since disturbances d_1 and d_2 , both previously assumed to be known in ideal steady-state signals, are in fact unknown and unmeasurable in practical applications, a set of disturbance observers is developed to reconstruct the disturbance information and use it during the controller synthesis. Therefore, based on [31], the following HOSMOs are designed

$$\text{for } d_1 : \begin{cases} \dot{z}_{1,0} = x_2 + f_1(\bar{\mathbf{x}}) + \Phi_{1,1}, z_{1,i} = \Phi_{1,i+1}, \\ \dot{h}_{1,i} = z_{1,i} - \Phi_{1,i}, \text{ for } i = 0, 1, 2, \\ \Phi_{1,1} = -\ell_{1,0}\lambda_1^{1/3}|\hbar_{1,0}|^{2/3}\text{sign}(\hbar_{1,0}) + z_{1,1}, \\ \Phi_{1,2} = -\ell_{1,1}\lambda_1^{1/2}|\hbar_{1,1}|^{1/2}\text{sign}(\hbar_{1,1}) + z_{1,2}, \\ \Phi_{1,3} = -\ell_{1,2}\lambda_1\text{sign}(\hbar_{1,2}); \end{cases} \quad (5)$$

$$\text{for } d_2 : \begin{cases} \dot{z}_{2,0} = u_1 + f_2(\bar{\mathbf{x}}) + C_1 + \Phi_{2,1}, \\ \dot{z}_{2,1} = \Phi_{2,2}, \hbar_{2,i} = z_{2,i} - \Phi_{2,i}, \text{ for } i = 0, 1, \\ \Phi_{2,1} = -\ell_{2,0}\lambda_2^{1/2}|\hbar_{2,0}|^{1/2}\text{sign}(\hbar_{2,0}) + z_{2,1}, \\ \Phi_{2,2} = -\ell_{2,1}\lambda_2\text{sign}(\hbar_{2,1}), \end{cases} \quad (6)$$

where $\Phi_{1,j+1}$, $\Phi_{2,i}$, $\hbar_{1,j}$, and $\hbar_{2,i-1}$ are the auxiliary states; $\Phi_{i,0} = x_i$; $z_{i,0}$ is the estimate of x_i ; $z_{1,1}$, $z_{1,2}$, and $z_{2,1}$ are the corresponding estimates of d_1 , \dot{d}_1 , and d_2 ; $\ell_{1,j}$, $\ell_{2,i-1}$, and λ_i are the positive gains where $i = 1, 2$ and $j = 0, 1, 2$.

Remark 1: Although HOSMOs can reconstruct unknown disturbances within a finite time, their tuning is not trivial. In

this context, the following empirical methodology of parameter selection is employed: a) Set $\ell_{1,j}$ and $\ell_{2,i-1}$ to relatively small values, such as 1 or 2, among which the relationships $\ell_{1,0} > \ell_{1,1} > \ell_{1,2}$ and $\ell_{2,0} > \ell_{2,1}$ are generally satisfied; b) Adjust λ_i from small to large until HOSMOs can effectively converge. Typically, λ_i inclines to be a relatively large value to enable the accurate estimation of disturbances; c) Fine-tuning of $\ell_{1,j}$, $\ell_{2,i-1}$, and λ_i is required until the desired estimation performance is obtained.

B. Optimal Controller Design

1) Steady-State Signals Construction: Substituting the disturbance estimates $z_{1,1}$, $z_{1,2}$, and $z_{2,1}$ into (3), the implementable reference trajectory signals can be formulated as

$$\begin{cases} \hat{x}_1^* = 0, \hat{x}_2^* = -z_{1,1}, \\ \hat{u}_1^* = -\frac{R_s}{L_s}z_{1,1} - z_{1,2} - z_{2,1} - C_1. \end{cases} \quad (7)$$

Define $\hat{\delta}_\omega = x_1 - \hat{x}_1^*$, $\hat{\delta}_q = x_2 - \hat{x}_2^*$, $\hat{v}_q = u_1 - \hat{u}_1^*$, and $\varepsilon_{i,1} = z_{i,1} - d_i$, $i = 1, 2$. Then, by incorporating (7) into system (4), one can arrive at

$$\begin{cases} \dot{\hat{\delta}}_\omega = \hat{\delta}_q + f_1(\bar{\mathbf{x}}) - f_1(\hat{\mathbf{x}}^*) + \zeta_1, \\ \dot{\hat{\delta}}_q = \hat{v}_q + f_2(\bar{\mathbf{x}}) - f_2(\hat{\mathbf{x}}^*) + \zeta_2, \end{cases} \quad (8)$$

where $\hat{\mathbf{x}}^* = (\hat{x}_1^*, \hat{x}_2^*)^\top$, $\zeta_1 = -\varepsilon_{1,1}$, $\zeta_2 = \Phi_{1,2} - z_{1,2} - \varepsilon_{2,1}$.

2) Receding-Horizon Optimization: At this stage, by ignoring the effects brought by tracking and estimation errors, the system nominal model can be expressed as

$$\dot{\hat{\delta}}_\alpha = \mathbf{A}\hat{\delta}_\alpha + \mathbf{B}\hat{v}_q, \quad (9)$$

$$\text{where } \hat{\delta}_\alpha = [\hat{\delta}_\omega, \hat{\delta}_q]^\top, \mathbf{A} = \begin{bmatrix} 0 & 1 \\ 0 & 0 \end{bmatrix}, \mathbf{B} = [0, 1]^\top.$$

In the case where the control order is chosen as zero (for the detailed definition of *control order* one can refer to [27]), within a period of τ , the future output signal $\tilde{\delta}_\omega(t+\tau)$ can be predicted via Taylor expansions along system (9) as

$$\tilde{\delta}_\omega(t+\tau) \doteq \hat{\delta}_\omega + \tau\hat{\delta}_q + \frac{\tau^2}{2!}\hat{v}_q = \bar{\mathbf{H}}\hat{\delta}_\alpha + \frac{\tau^2}{2!}\hat{v}_q, \quad (10)$$

where $\bar{\mathbf{H}} = [1, \tau]$.

For the purpose of regulating tracking error signals $\hat{\delta}_\omega$ so that they can optimally converge to the origin, the following cost function (to be optimized) can be defined

$$\hat{J}_\alpha = \frac{1}{2} \int_0^{T_1} \tilde{\delta}_\omega^2(t+\tau) d\tau, \quad (11)$$

where T_1 is the prediction horizon.

By substituting (10) into (11), one obtains

$$\hat{J}_\alpha = \hat{\delta}_\alpha^\top \bar{\mathbf{H}}_1 \hat{\delta}_\alpha + \hat{\delta}_\alpha^\top \bar{\mathbf{H}}_2 \hat{v}_q + \frac{1}{2} \bar{\mathbf{H}}_3 \hat{v}_q^2. \quad (12)$$

$$\text{where } \bar{\mathbf{H}}_1 = \begin{bmatrix} \frac{T_1}{2} & \frac{T_1^2}{2} \\ \frac{T_1^2}{4} & \frac{T_1^3}{6} \end{bmatrix}, \bar{\mathbf{H}}_2 = \begin{bmatrix} \frac{T_1^3}{6} & \frac{T_1^4}{8} \end{bmatrix}^\top, \bar{\mathbf{H}}_3 = \frac{T_1^5}{20}.$$

To minimize the performance index \hat{J}_α , one can take its partial derivative with respect to \hat{v}_q , which yields

$$\frac{\partial \hat{J}_\alpha}{\partial \hat{v}_q} = \bar{\mathbf{H}}_2^\top \hat{\delta}_\alpha + \bar{\mathbf{H}}_3 \hat{v}_q. \quad (13)$$

Letting $\frac{\partial \hat{J}_\alpha}{\partial \hat{v}_q} = 0$ derives the optimal control law as

$$\hat{v}_q = -\bar{\mathbf{H}}_3^{-1}\bar{\mathbf{H}}_2^\top\hat{\delta}_\alpha = -\frac{k_\omega^*}{T_1^2}\hat{\delta}_\omega - \frac{k_q^*}{T_1}\hat{\delta}_q, \quad (14)$$

where $k_\omega^* > 0$ and $k_q^* > 0$, both rendered from $\bar{\mathbf{H}}_3^{-1}\bar{\mathbf{H}}_2^\top$.

Remark 2: In the conventional GPC scheme, the horizon in the optimal control law (14) is commonly configured as fixed values via engineering experience. However, by this means, the performance optimization of the system may exhibit deviation behavior under some drastically varied operation conditions. As a specific example in electric vehicles, the desired speed for PMSM drives generally needs to be regulated over a wide range, including different levels of step speed changes and loads. It is clear that the fixed horizon configuration is unable to provide a solid performance optimization in the allowable operating conditions.

3) *Self-Tuning Horizon Mechanism Design:* To offer an alternative solution to address the aforementioned limitations of the GPC employing a fixed horizon, a self-tuning mechanism based on the horizon T_1 is developed as follows

$$\begin{cases} T_1 = \frac{T_0}{l_q}, \quad T_0 > 0, \\ \dot{l}_q = \rho \frac{\hat{\delta}_\omega^2}{l_q^2} (1 + \text{sign}(|\hat{\delta}_\omega| - \delta_s)), \\ l_q = 1, \quad \omega_{\text{ref}}(k) \neq \omega_{\text{ref}}(k-1), \end{cases} \quad (15)$$

where T_0 is the initial value of T_1 , ρ is the positive scaling gain, l_q is the bandwidth factor, δ_s is the error threshold, and $\omega_{\text{ref}}(k)$ represents the reference speed at the moment k .

With (15) in mind, it is clear that different ranges of speed regulation will result in l_q converging to different values from the initial condition. This implies that different prediction horizons could be captured for different operating conditions. In scenarios with broader speed switching, l_q converges to a larger value, indicating the preference for a lower T_1 to maintain transient performance, as confirmed by the results shown in Fig. 9 of Section VI.C. Moreover, when ω_{ref} changes, l_q will be reset to 1, allowing the reconfiguration of the appropriate horizon to match the current operating condition.

4) *Composite Optimized Controller Design:* Subsequently, the terminal optimal speed controller combined with the self-tuning horizon mechanism (15) can be derived as

$$u_{cq} = \frac{2JL_s}{3n_p\psi_f} \left(\frac{k_\omega^*}{T_1^2}\hat{\delta}_\omega + \frac{k_q^*}{T_1}\hat{\delta}_q - \hat{u}_1^* \right). \quad (16)$$

Remark 3: The guideline for parameter setting of the proposed GDPC algorithm is quite straightforward and can be summarized as follows:

- 1) Firstly, according to (11)-(14), the optimal control gains k_ω^* and k_q^* can be derived directly from the receding horizon optimization procedure;
- 2) Secondly, the scaling gain ρ and the initial value T_0 can be chosen via a trial-and-error approach, and the details of their selection one can be referred to Section VI.B;
- 3) Thirdly, to avoid the uncontrollable decrease of T_1 , δ_s as the error threshold is introduced to shield the increase of l_q at $|\hat{\delta}_\omega| < \delta_s$, which can be selected by observing the actual fluctuation of $\hat{\delta}_\omega$.

C. Current and Voltage Constraints

To tackle the current protection concern arising from the adoption of the non-cascade structure, a current constraint design based on model predictive approach is introduced in this paper, drawing inspiration from [32]. With $i_d^* = 0$ strategy employed, and assuming that d -axis current controller works well, the current constraint can be formulated as

$$-I_{\max} \leq i_q(t) \leq I_{\max}, \quad (17)$$

where I_{\max} is the maximum allowable current, often chosen to be 2 to 3 times the rated current in industrial applications [26].

Firstly, a simple transformation of system (2) yields the following q -axis voltage equation with matched disturbance

$$u_q(t) = L_s \dot{i}_q(t) + R_s i_q(t) + e_q(t) + C_2 d_2(t), \quad (18)$$

where $e_q(t) = n_p \omega(t) (L_s i_q(t) + \psi_f)$ and $C_2 = \frac{2JL_s}{3n_p\psi_f}$.

Subsequently, by replacing d_2 with its estimated value $z_{2,1}$, and applying zero-order hold discretization T_s [33], the discrete form of (18) can be obtained

$$u_q(n) = \frac{1}{\vartheta} i_q(n+1) - \frac{\chi}{\vartheta} i_q(n) + e_q(n) + C_2 z_{2,1}(n), \quad (19)$$

where T_s is the sampling period, $\vartheta = \frac{1}{R_s} (1 - e^{-T_s R_s / L_s})$ and $\chi = e^{-T_s R_s / L_s}$.

Based on (17) and (19), the boundary values of the q -axis voltage required to restrict i_q within a safe range of $[-I_{\max}, I_{\max}]$ can be derived as

$$\begin{cases} u_{i_max}(n) = \frac{1}{\vartheta} I_{\max} - \frac{\chi}{\vartheta} i_q(n) + e_q(n) + C_2 z_{2,1}(n), \\ u_{i_min}(n) = -\frac{1}{\vartheta} I_{\max} - \frac{\chi}{\vartheta} i_q(n) + e_q(n) + C_2 z_{2,1}(n), \end{cases} \quad (20)$$

where u_{i_max} and u_{i_min} are the maximum and minimum q -axis voltage values that satisfy current constraint (17).

With (20) in mind, current constraint (17) can be transformed into the following voltage constraint

$$u_{i_min}(n) \leq u_q \leq u_{i_max}(n). \quad (21)$$

Meanwhile, according to the d -axis voltage u_d derived from d -axis current controller, q -axis voltage u_q needs to satisfy the following voltage constraint

$$u_{v_min}(n) \leq u_q \leq u_{v_max}(n), \quad (22)$$

where $u_{v_max}(n) = -u_{v_min}(n) = \sqrt{V_{\max}^2 - u_d(n)^2}$ and V_{\max} is the maximum voltage limited by inverter and motor.

Therefore, to guarantee that both the voltage and current constraints are respected, the q -axis voltage u_{cq} generated by our proposed controller (16), must meet

$$u_{\min}(n) \leq u_{cq} \leq u_{\max}(n), \quad (23)$$

where $u_{\min}(n) = \max\{u_{v_min}(n), u_{i_min}(n)\}$ and $u_{\max}(n) = \min\{u_{v_max}(n), u_{i_max}(n)\}$.

Remark 4: It should be noted that the literature [32] does not take into account the matched disturbance in the system. Consequently, deviations in the current constraint may occur when the system undergoes unmodeled dynamics or

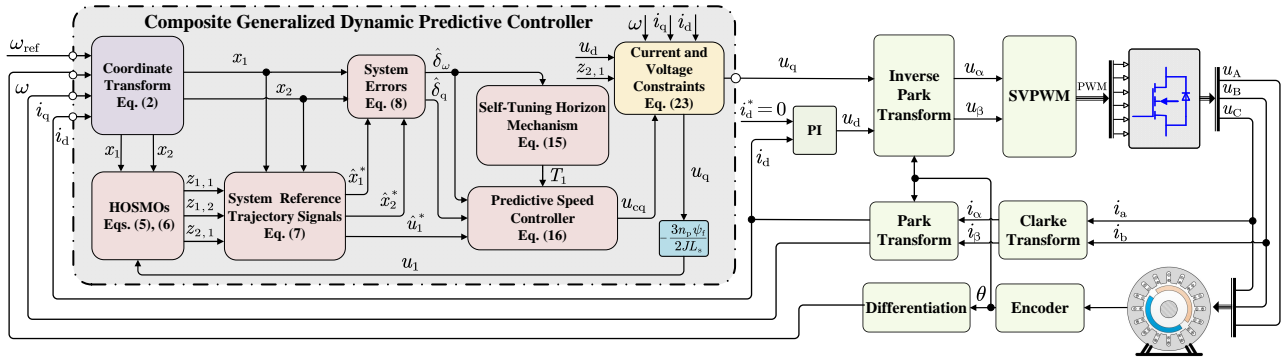


Fig. 1. The framework of the proposed composite GDPC with a self-tuning horizon.

parametric perturbations. To address this issue, the disturbance compensation technique is employed in this article to incorporate disturbance estimation information into (18), thereby enhancing the control system robustness against disturbance. To sum up, the detailed design framework of the proposed composite GDPC approach is shown in Fig. 1.

Theorem 1: For the PMSM system (1), with appropriate selections of the control parameters T_0 , ρ , and the observer parameters λ_i , $\ell_{i,j}$, the closed-loop system comprising the HOSMOS (5), (6), the composite predictive speed controller (16), the self-tuning horizon mechanism (15), and the constraints handling mechanism (23), will yield the following conclusions:

- 1) The closed-loop system is asymptotically stable when (23) is inactive, i.e., $u_{cq} \in [u_{\min}, u_{\max}]$.
- 2) The closed-loop system is bounded when (23) is activated, i.e., $u_{cq} \notin [u_{\min}, u_{\max}]$.

Proof: For readability, the thorough stability analysis is given in the Appendix.

IV. DISCUSSIONS AND EXTENSIONS

In this section, based on existing methods, the important basic control requirements are extended with a minor modification of the proposed control framework depicted in Fig. 1.

A. Extension to Interior PMSMs

Different from SPMSM, the d -axis and q -axis inductances of interior PMSM (IPMSM) are not equal. Based on the physical model of IPMSM in the d - q frame [34], by defining $x_1 = \omega - \omega_{\text{ref}}$ and $x_2 = -\frac{3n_p}{2J}\phi(i_d)i_q + \frac{B_m}{J}\omega_{\text{ref}}$ as the system states where $\phi(i_d) = (L_d - L_q)i_d + \psi_f$, L_d and L_q are the d -axis and q -axis stator inductances, one can easily obtain a state-space model of the IPMSM system similar to system (2) by letting $i_d = 0$, with

$$f_1(\bar{x}) = -\frac{B_m}{J}x_1, C_1 = \frac{1}{JL_q}(R_s B_m + \frac{3}{2}n_p^2 \psi_f \phi) \omega_{\text{ref}},$$

$$f_2(\bar{x}) = -\frac{3n_p^2 \psi_f \phi}{2JL_q}x_1 - \frac{R_s}{L_q}x_2 + \frac{3n_p^2 \phi L_d}{2JL_q}(\omega_{\text{ref}} - x_1)i_d.$$

Among the existing speed control approaches for IPMSM drives, they can be broadly categorized into two main strategies: i) FOC with $i_d^* = 0$ [35], and ii) maximum torque per ampere (MTPA) strategy [36].

1) *FOC with $i_d^* = 0$:* In this strategy, i_d^* is set to zero, resulting in the electromagnetic torque being directly proportional to the q -axis current [37]. Meanwhile, based on the state-space model of IPMSM and following the design procedures presented in Section III, a composite generalized dynamic predictive speed controller for the IPMSM system can be designed. Hence, under this strategy, the proposed control framework depicted in Fig. 1, can be directly used for speed regulation of IPMSM drives with a redesign of the controller based on the proposed GDPC methodology.

2) *MTPA strategy:* Distinct from $i_d^* = 0$ strategy discussed above, the MTPA strategy aims to minimize the stator current for the desired torque generation. In this strategy, the relationship between i_d and i_q can be deduced as [38]

$$i_d = \frac{\psi_f}{2(L_q - L_d)} - \sqrt{\frac{\psi_f^2}{4(L_q - L_d)^2} + i_q^2}. \quad (24)$$

Fig. 2 depicts the control block diagram for speed regulation of IPMSM drives using the proposed control scheme under MTPA operation. Firstly, similar to $i_d^* = 0$ strategy, a composite generalized dynamic predictive speed controller for IPMSM is designed based on the established state-space model of IPMSM, utilizing our proposed approach. Secondly, the MTPA strategy presented in [39] is employed to modify the d -axis current reference i_d^* by (24) combining q -axis current feedback i_q , enabling the realization of optimal current trajectories and enhancing the efficiency of torque output for IPMSM. It is easy to see that the framework shown in Fig. 2 is essentially a minor extension of our proposed control framework, with the addition of the MTPA algorithm to modify the i_d^* component.

B. Extension to Flux-Weakening Operation

Considering that in certain specific applications, such as electric propulsion, spindle drives and electric vehicles, a wider speed range is required, which necessitates the operation to be extended from constant torque region to constant power region. Fig. 3 presents a flux-weakening control (FWC) framework for IPMSM drives based on our proposed approach. Under this framework, as illustrated in Fig. 4, the flux-weakening control component described in [40] is seamlessly incorporated into the proposed control framework.

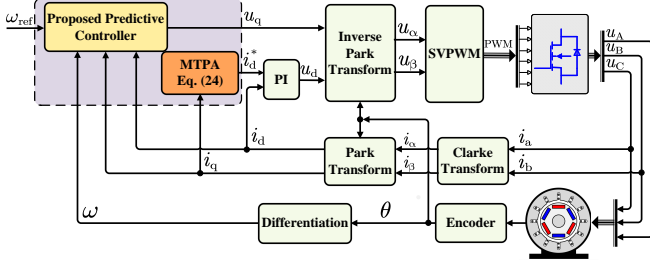


Fig. 2. Overall diagram of IPMSM utilizing the proposed control scheme under MTPA operation.

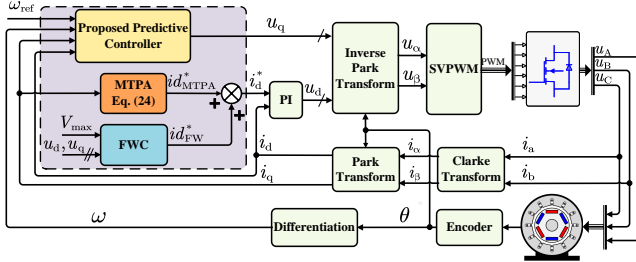
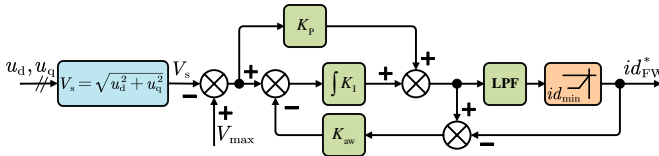


Fig. 3. Control diagram for IPMSM drives based on the proposed control scheme with flux-weakening control loop.



This component involves a PI controller, supported by a low-pass filter (LPF) and an anti-windup structure, to modify the d -axis current reference i_d^* . It is important to note that this framework is also applicable to SPMMSM by setting i_d^* to zero.

Below the base speed, the magnitude of the voltage vector V_s ($V_s = \sqrt{u_d^2 + u_q^2}$) is typically less than V_{max} (defined as the maximum voltage limited by inverter and motor). The flux-weakening control remains inactive at this point, and the motor operates in MTPA mode within constant torque region. As speed increases and the output voltage is outside the voltage limit circle or ellipse, autonomous activation of the flux-weakening operation takes place. In flux-weakening mode, a negative d -axis current reference, denoted as i_d^{*FW} , is generated to decrease the flux in the stator windings. This action frees up a portion of voltage, allowing the motor to operate in the high-speed region.

V. SIMULATION VERIFICATION

In order to validate the performance improvement of the proposed methodology, simulation tests are conducted using MATLAB/Simulink, while evaluating the execution time of the methods involved.

In this simulation, the single-loop MPC based on disturbance observer in [19], the baseline GPC in [27], and the classical cascade PI are considered as benchmark methods for comparison. Meanwhile, the selection of control parameters comprehensively considers the dynamic performance,

current response and disturbance rejection capability of the system. The control parameters are set as follows: MPC: $T_s = 5 \times 10^{-5}$, $N_p = 20$, $N_c = 3$, $Q = 500I_{20 \times 20}$, $R = 1.5$, $\ell_{1,0} = 2$, $\ell_{1,1} = 1.2$, $\lambda_1 = 4800$, $\ell_{2,0} = 4$, $\ell_{2,1} = 1.5$, $\lambda_2 = 9.5 \times 10^3$; Cascade PI: $k_{vp} = 0.0549$, $k_{vi} = 2.4 \times 10^{-4}$ for the speed loop, $k_{pp} = 3.46$, $k_{pi} = 0.315$ for the current loop; GDPC: $T_0 = 1.1$, $\rho = 70$, $\delta_s = 3$, $\ell_{1,0} = 4$, $\ell_{1,1} = 2$, $\ell_{1,2} = 1.1$, $\lambda_1 = 15500$, $\ell_{2,0} = 5$, $\ell_{2,1} = 2$, $\lambda_2 = 1.2 \times 10^6$, $k_{\omega}^* = 10/3$, $k_q^* = 2.5$; GPC: $T_1 = 0.004$, the remaining parameters are the same as in GDPC; the d -axis current controller: $k_{dp} = 3.46$, $k_{di} = 0.315$.

As shown in Fig. 5, the proposed GDPC, the traditional GPC and MPC exhibit similar dynamic performance, with a speed change from 500 to 1500 rpm at $t = 1$ s, except for the PI which has a large overshoot. A constant load of 0.08 Nm is then applied to the motor at $t = 1.5$ s. It can be observed that the proposed GDPC showcases rapid performance recovery and minimal speed drop, with the GPC and the MPC following closely, while the PI exhibits the least favorable performance.

In parallel, the execution time of the control algorithms involved is evaluated through the Simulink Profiler tool in MATLAB/Simulink, and the results are listed in Table I. It can be seen that the PI has the shortest execution time and the proposed GDPC and GPC have comparable execution efficiency, slightly higher than the PI. However, the execution time of the MPC is significantly greater than the other three approaches, owing to the necessity of solving the optimal problem in each control iteration. This confirms that the proposed method incurs only a marginal computational burden compared to the MPC. Consequently, the real-time performance of the proposed controller is easier to ensure in practical applications.

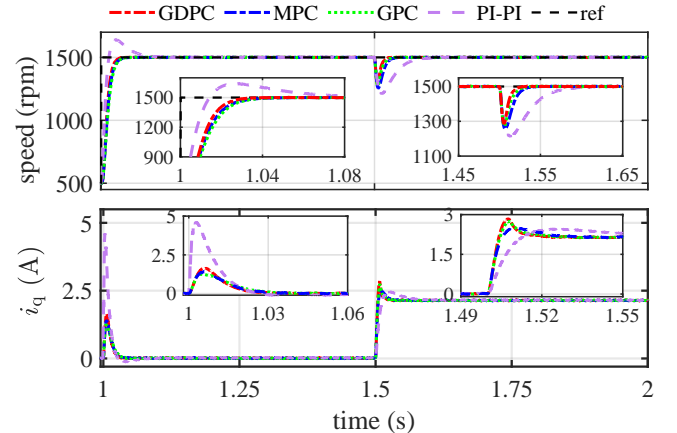


Fig. 5. System response curves for the cascade PI, the GPC, the MPC and the proposed GDPC.

TABLE I
COMPARISON OF CALCULATION EFFICIENCY

Controller	Total time (s)	Time of each control cycle (μ s)
PI-PI	0.141	3.525
GPC	0.421	10.525
GDPC	0.51	12.75
MPC	4.751	118.77

VI. EXPERIMENTAL RESULTS

To further verify the effectiveness of the proposed methodology, a series of experiments are performed on a digital signal processor (DSP)-based PMSM drive system.

A. Experimental Setup

The experimental setup, depicted in Fig. 6, consists of a control unit (F28379d) and two driver boards (DRV8305), all manufactured by Texas Instruments. The F28379d is equipped with two CPU cores, each operating at 200MHz. CPU1 functions as the main controller, operating the drive motor in speed mode and interacting with the host PC for data exchange. Meanwhile, CPU2 serves as the auxiliary controller to operate the load motor in torque mode for expected torque generation, which acts as a load on the drive motor. Communication between the CPUs is realized via the internal IPC module. The control algorithm is developed in MATLAB/Simulink using the model-based design methodology. The parameters of the two adopted SPMSMs are specified in Table II. The sampling frequency is set as 20KHz.

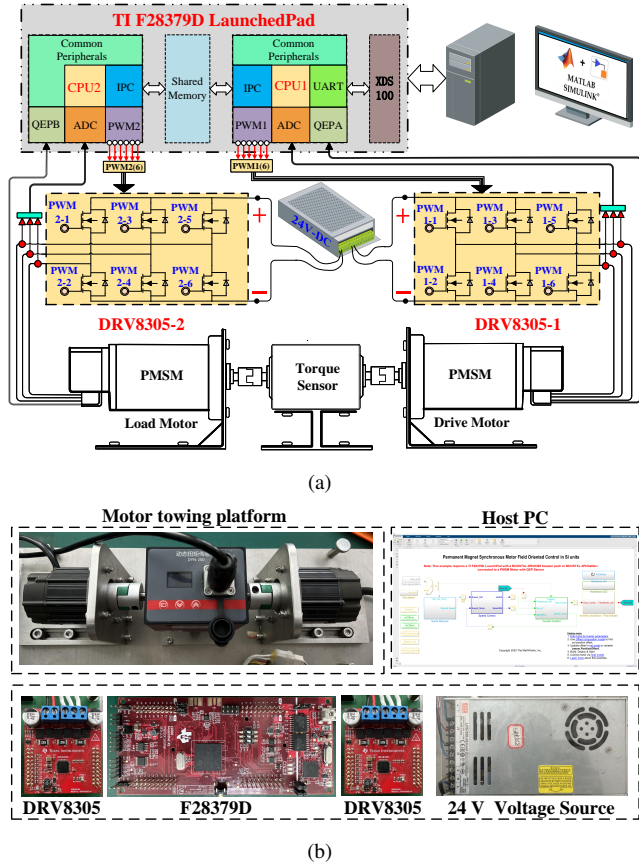


Fig. 6. Experimental setup: (a) Connection diagram. (b) Used components.

B. Parameters Selection

In order to clarify the principle behind control parameter selection in the proposed composite GDPC approach, a series of experiments with different ρ and T_0 are carried out on the SPMSM speed regulation system. For a comprehensive

TABLE II
PARAMETERS OF THE USED SPMSM DRIVE

Symbol	Meaning	Nominal value & unit
n_p	Poles	4
R_s	Stator resistance	0.36Ω
L_s	Stator inductance	$2.0 \times 10^{-4} \text{ H}$
ψ_f	Flux linkage	0.0064 Wb
J	Rotor inertia	$7.066 \times 10^{-6} \text{ kg}\cdot\text{m}^2$
B_m	Viscous damping	$2.637 \times 10^{-6} \text{ N}\cdot\text{m}\cdot\text{s}/\text{rad}$
ω_n	Rated speed at V_{dc}	4107 rpm
ω_{max}	Maximum speed	6000 rpm
I_N	Rated current	7 A
I_{max}	Peak current	20 A
V_{dc}	Bus voltage	24 V

analysis, the test condition included a speed step from 500 to 2000 rpm at $t = 8$ s, a constant load of 0.12 Nm at $t = 10$ s, and a time-varying load of $0.12\sin(2\pi t)$ Nm at $t = 12$ s.

It is observed from Fig. 7 that selecting a larger value for ρ results in a faster response and increased robustness to the load disturbance. However, an excessively large ρ may lead to undesired speed overshoot and high peak q -axis current. Therefore, ρ generally needs to be selected from small to large until the expected performance is obtained. Additionally, as shown in Fig. 8, selecting a smaller T_0 also enhances response speed and disturbance rejection capability. However, too small T_0 will lead to the same issue encountered with ρ . Consequently, a compromise is necessary to strike a balance between dynamic performance and disturbance rejection ability by choosing appropriate ρ and T_0 .

TABLE III
DESIGN OF TEST WORKING CONDITIONS

Time	Case 1	Case 2	Case 3
$t=8$ s	500 to 1500 rpm	500 to 3000 rpm	500 to 4000 rpm
$t=10$ s	$T_L=0.2$ Nm	$T_L=0.2$ Nm	$T_L=0.05$ Nm
$t=12$ s	$T_L=0.2\sin(2\pi t)$ Nm	$T_L=0.2\sin(3\pi t)$ Nm	$T_L=0.05\sin(4\pi t)$ Nm

C. Performance Verification

To further verify the effectiveness of the proposed control approach in light of the already existing methods, the cascade PI, the LADRC [14], and the baseline GPC with both low and large horizons [27] are chosen as the comparative controllers. Among them, except for the PI, the others are based on a non-cascade structure. The different experimental scenarios are listed in Table III. To ensure a fair comparison, the controller parameter tuning takes into account the system stability, dynamic performance, peak current, and robustness against disturbance, utilizing the trial and error method. The controller parameters are selected as follows: Cascade PI: $k_{vp} = 0.0916$, $k_{vi} = 3.63 \times 10^{-4}$ for the speed loop, $k_{pp} = 3.46$, $k_{pi} = 0.315$ for the current loop; LADRC: $\omega_o = 1200$, $\omega_c = 400$, $b_0 = \frac{3n_p\psi_f}{2JL_s}$; GDPC: $T_0 = 1.3$, $\rho = 40$, $\delta_s = 3$, $\ell_{1,0} = 14$, $\ell_{1,1} = 4.5$, $\ell_{1,2} = 3$, $\lambda_1 = 5500$, $\ell_{2,0} = 7$, $\ell_{2,1} = 4$, $\lambda_2 = 4.5 \times 10^8$, $k_w^* = 10/3$, $k_q^* = 2.5$; GPC (large): $T_1 = 4.5 \times 10^{-3}$, the remaining parameters are consistent with those in GDPC; GPC (low): $T_1 = 2.5 \times 10^{-3}$,

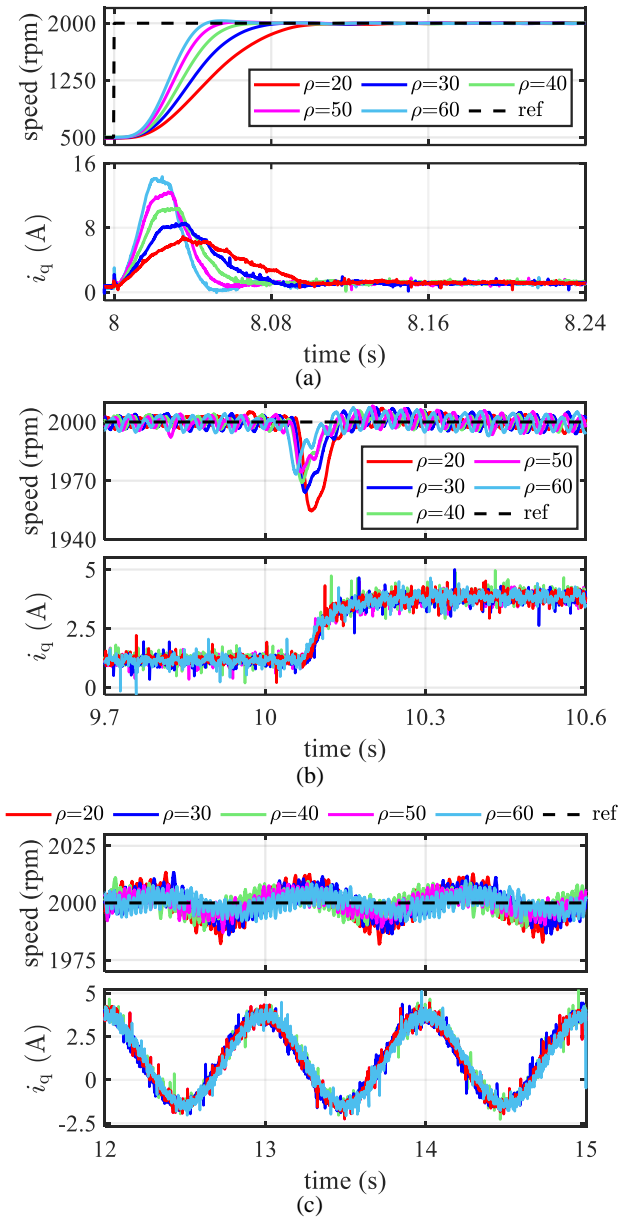


Fig. 7. Response curves of the proposed GDPC with different ρ subjected to three working conditions. (a) Speed switching. (b) Constant disturbance. (c) Time-varying disturbances.

the remaining parameters are consistent with those in GDPC; the d -axis current controller: $k_{dp} = 3.46$, $k_{di} = 0.315$.

1) *Disturbance Estimations and Self-Tuning*: Fig. 9 depicts the estimated disturbances by HOSMOs, and the response of the adaptive bandwidth factor l_q under three test cases. As the speed regulation range increases, the magnitude of matched disturbance estimate $z_{2,1}$ also grows, resulting in an increase in l_q such that lower T_1 be found to maintain the optimal performance. Moreover, the imposed mismatched load disturbance and its first-order derivative information are efficiently estimated for all three test cases.

2) *Dynamic Performance*: As shown in Fig. 10, the proposed GDPC consistently exhibits the best transient performance compared to the other two methods in all three cases. Furthermore, Fig. 11 illustrates that in Case 1, the response

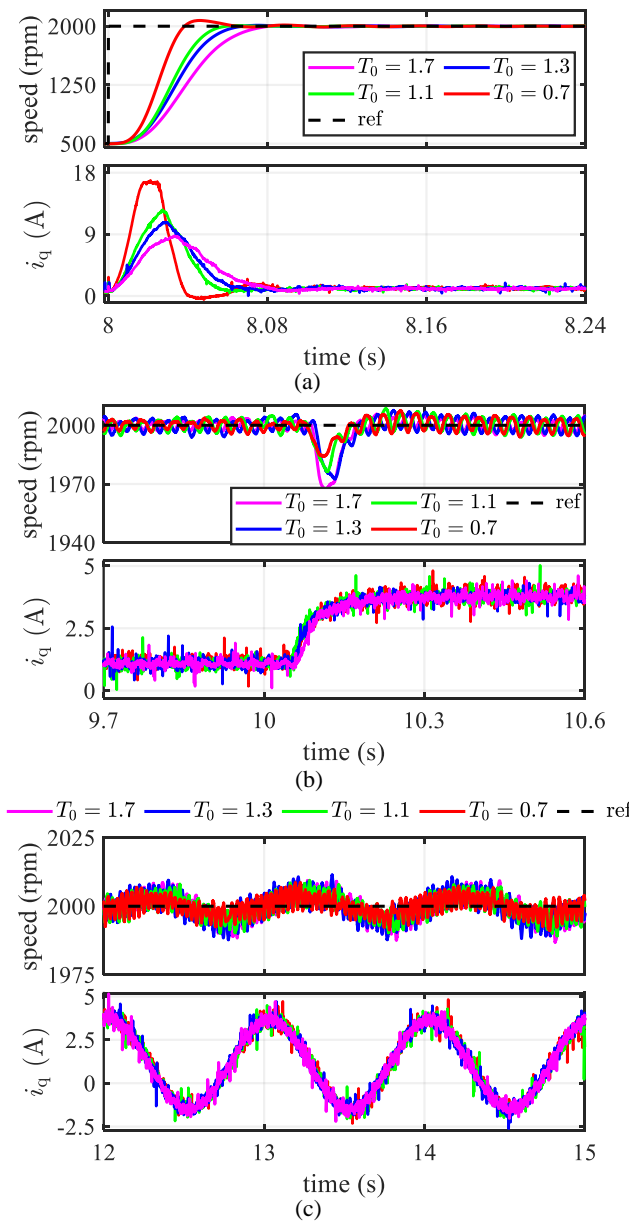


Fig. 8. Response curves of the proposed GDPC with different T_0 subjected to three working conditions. (a) Speed switching. (b) Constant disturbance. (c) Time-varying disturbances.

speed of the GPC (low) surpasses that of the proposed GDPC. However, thanks to the designed self-tuning horizon mechanism, which dynamically adjusts the horizon T_1 according to operating conditions, the GDPC shows superior dynamic performance to the GPC (low) in Cases 2 and 3. The GPC (large) displays the slowest response speed in all three cases. In both Cases 2 and 3, with a wide speed change initiated, the system encounters voltage saturation during the transient phase, causing a degree of current chattering.

3) *Constant Disturbance Rejection Performance*: As depicted in Fig. 12, when subjected to a constant external torque load, the cascade PI suffers the most significant speed drop, followed by the LADRC. In contrast, the proposed GDPC shows the lowest speed drop and the fastest performance recovery. Meanwhile, in Fig. 13, it can be observed that the

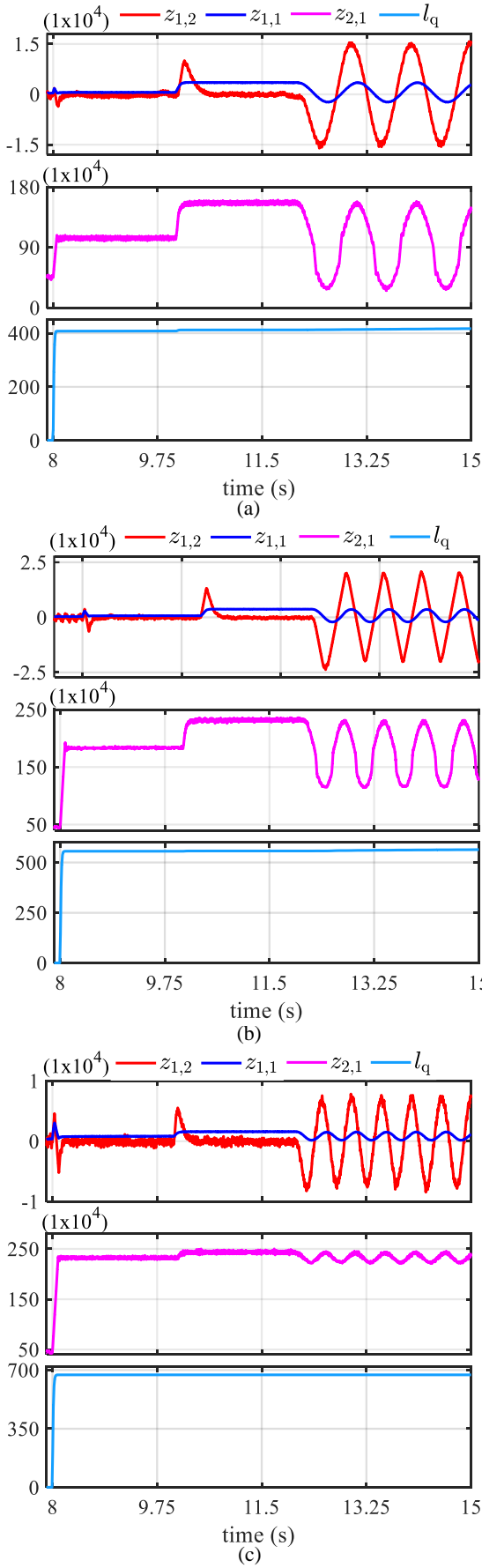


Fig. 9. Disturbance estimates by HOSMOs and response curves of l_q under three cases. (a) Case 1. (b) Case 2. (c) Case 3.

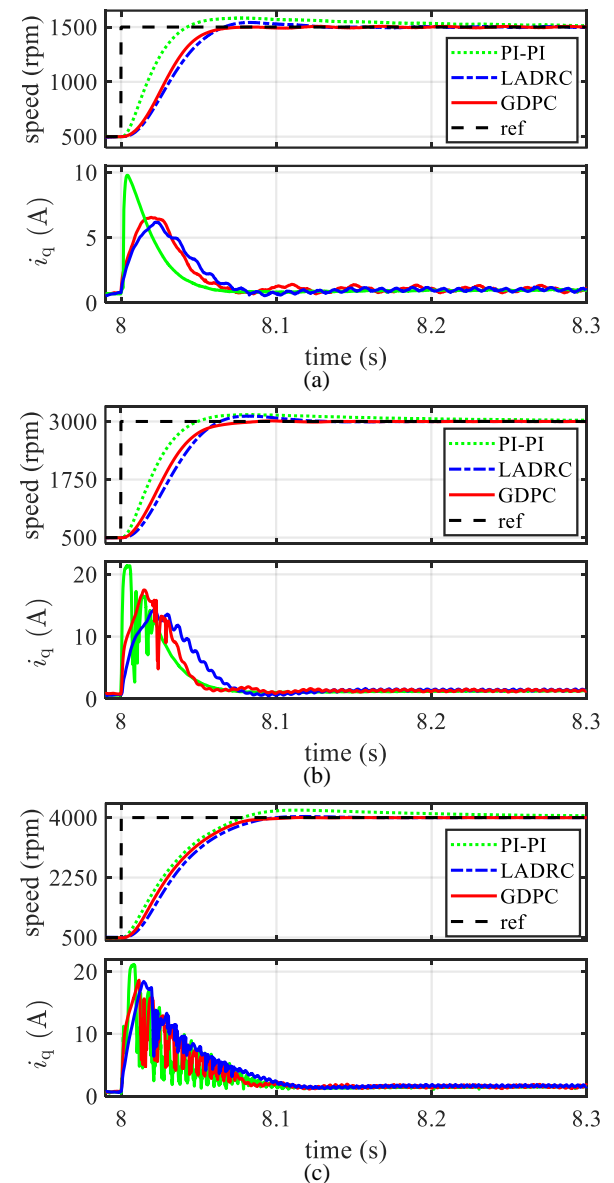


Fig. 10. Speed and q-axis current response curves for the cascade PI, the LADRC, and the GDPC methods, under three cases. (a) Case 1. (b) Case 2. (c) Case 3.

GPC (low) exhibits a speed drop similar to the GDPC in Case 1. However, in Cases 2 and 3, the speed drop of the GDPC is lower than that of the GPC (low), exhibiting a stronger capability to mitigate mismatched disturbance. Compared to the GPC (low) and the GDPC, the GPC (large) encounters the largest speed drop under all three test cases.

4) Time-varying Disturbance Rejection Performance: As can be seen from Fig. 14, when the system is subjected to a time-varying external load, both the cascade PI and the LADRC suffer from considerable speed fluctuations. In contrast, the proposed GDPC has significantly more small speed fluctuations than the two approaches. Furthermore, as seen in Fig. 15, the speed fluctuations of the GPC (low) and the proposed GDPC are similar in Case 1. However, in Cases 2 and 3, the GDPC shows less speed fluctuation than the GPC (low), effectively mitigating the adverse effect caused by the external

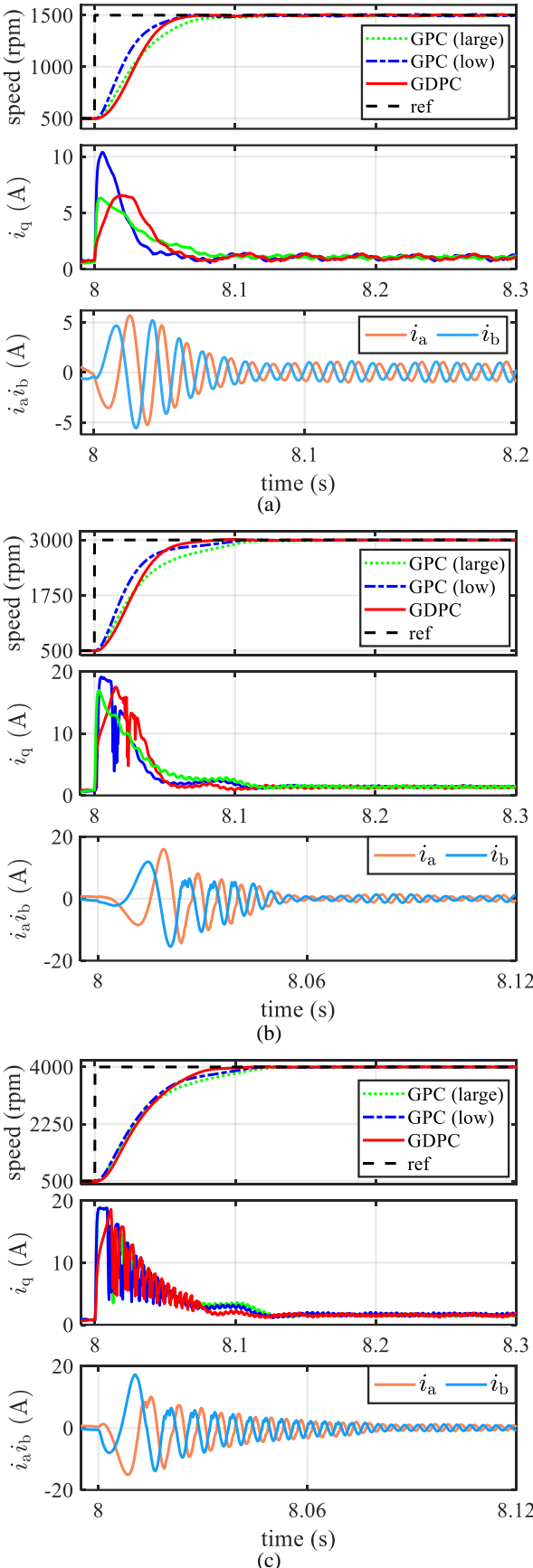


Fig. 11. Speed and q-axis current response curves for the GPC (large/low) and the GDPC methods, along with stator current response curves of the GDPC, under three cases. (a) Case 1. (b) Case 2. (c) Case 3.

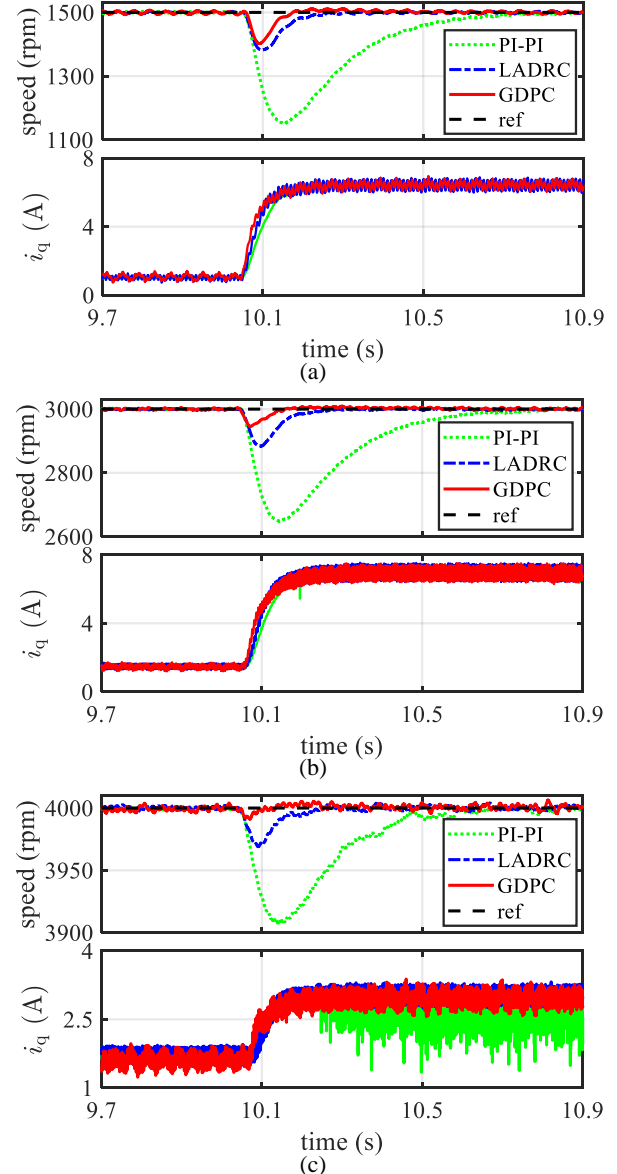


Fig. 12. Speed and q-axis current response curves for the cascade PI, the LADRC, and the GDPC methods, under three cases with the presence of a constant disturbance. (a) Case 1. (b) Case 2. (c) Case 3.

time-varying load. Among the three test cases, the GPC (large) is the most susceptible to mismatched disturbance brought by the time-varying load, in contrast to the GPC (low) and the proposed GDPC.

5) Robustness Against Parameter Perturbation: To validate the effectiveness of the proposed approach in addressing parameter perturbation, a series of experiments are performed with the system under different values of J . Specifically, the following test conditions are applied to provide a comprehensive analysis: a speed step from 500 to 2000 rpm at $t = 8$ s, a constant load of 0.2 Nm at $t = 10$ s, and a time-varying load of $0.2 \sin(2\pi t)$ Nm at $t = 12$ s. As depicted in Fig. 16, when the system is operated with a small J , it leads to a slight reduction in response speed and disturbance rejection capability. Conversely, when the system is subjected to a large J , the opposite effect is observed. Overall, this demonstrates

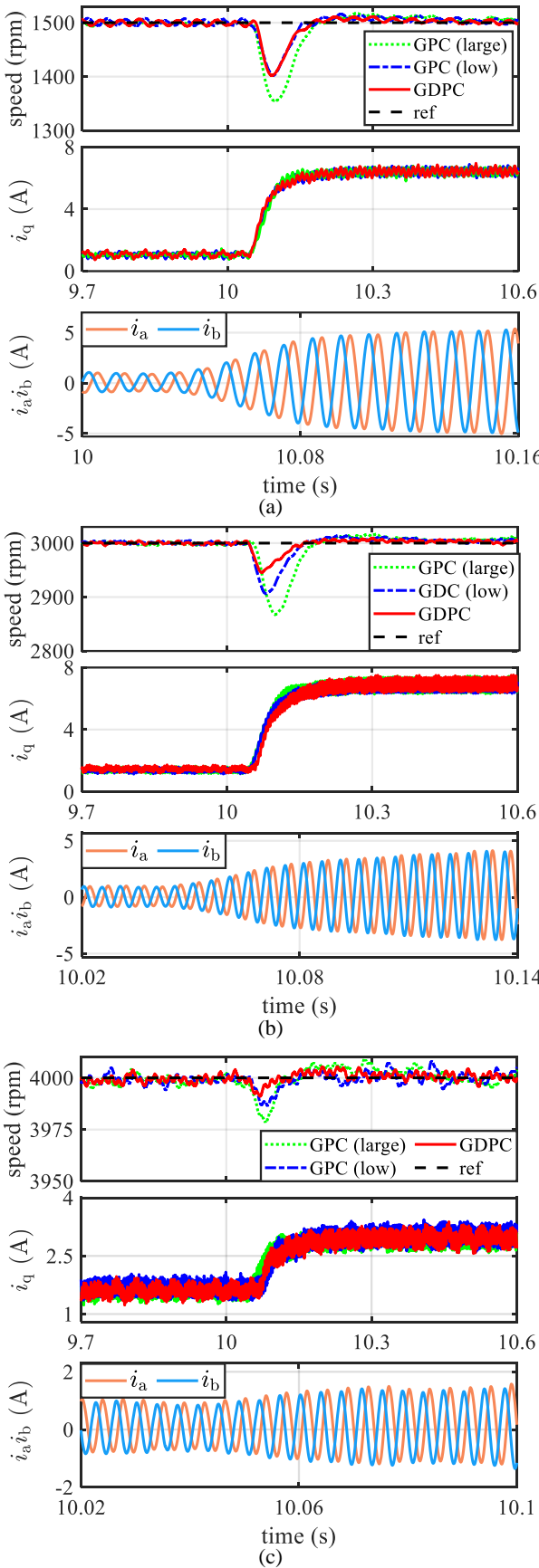


Fig. 13. Speed and q-axis current response curves for the GPC (large/low) and the GDPC methods, along with stator current response curves of the GDPC, under three cases with the presence of a constant disturbance. (a) Case 1. (b) Case 2. (c) Case 3.

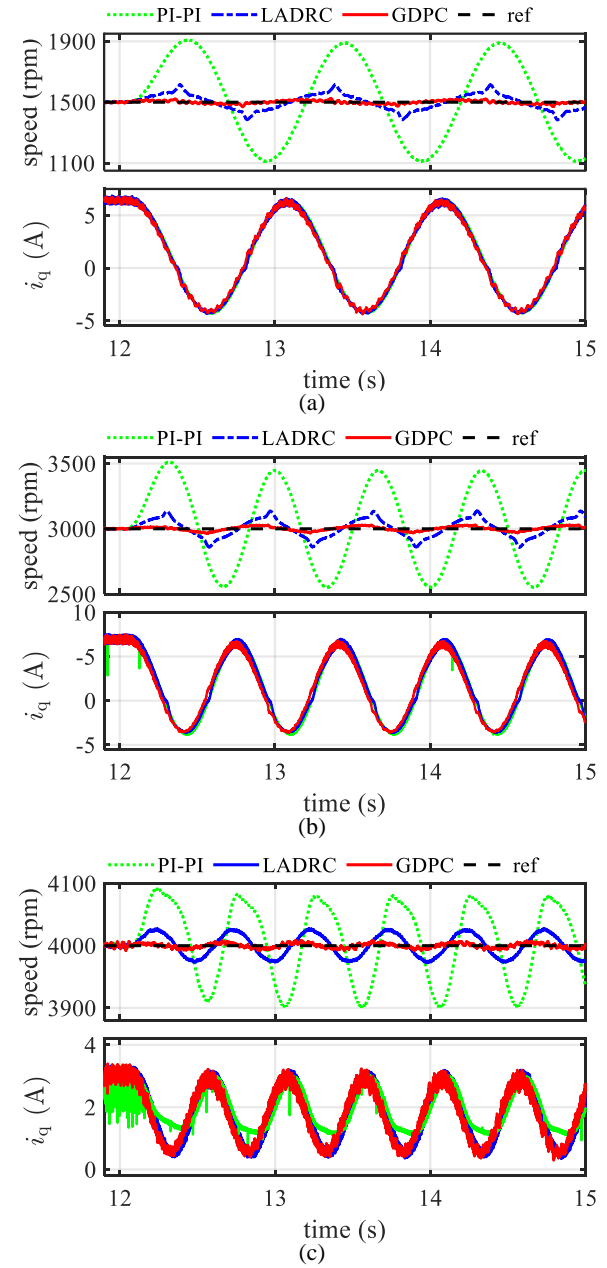


Fig. 14. Speed and q-axis current response curves for the GPC (large/low) and the GDPC methods under three cases with the presence of time-varying disturbances. (a) Case 1. (b) Case 2. (c) Case 3.

that the control performance of the closed-loop system based on the proposed approach can be effectively maintained, even within a certain range of parameter variations.

To provide a more intuitive analysis of the comparison, the performance indices for all the control methods involved under three test cases, including speed overshoot (OS), speed drop (SD), and speed fluctuations (SF), are presented in Table IV. Furthermore, Fig. 17 illustrates the performance indices of the proposed GDPC, GPC (low) and the GPC (large), which include the settling time, the mean square error (MSE) at 9.5–10.5 s, and the MSE at 11.5–14.8 s, under three test cases. To facilitate comparison, the MSEs have been normalized. From the above results, it can be concluded that under wide-range

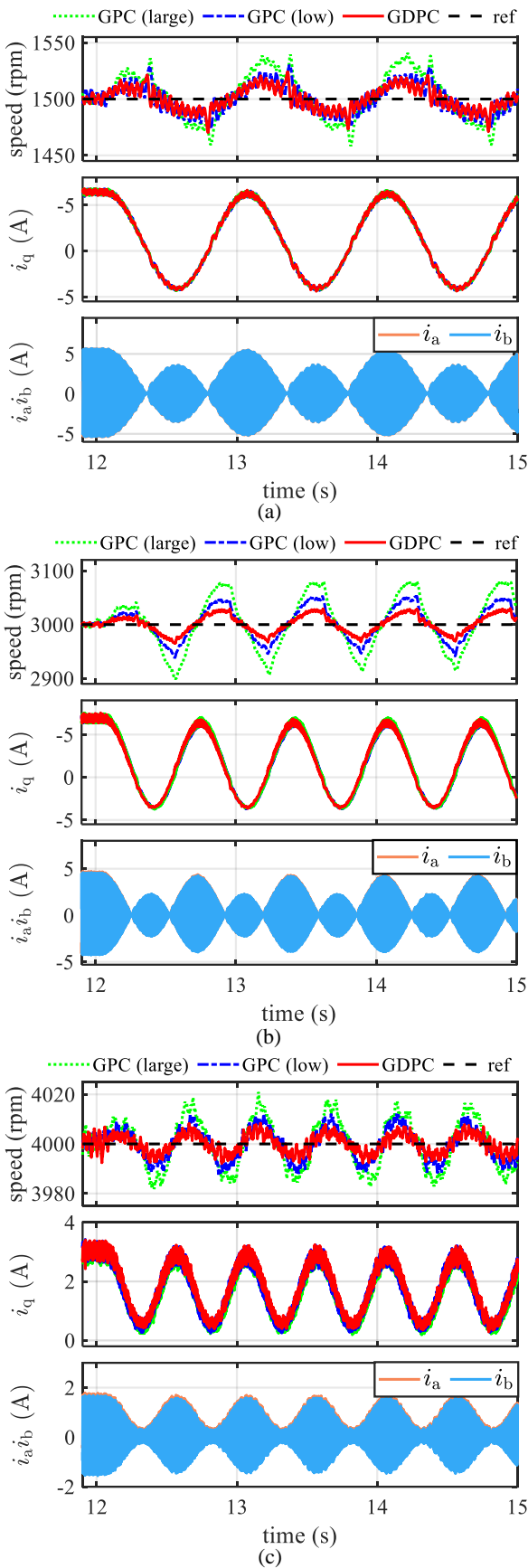


Fig. 15. Speed and q-axis current response curves for the GPC (large/low) and the GDPC methods, along with stator current response curves of the GDPC, under three cases with the presence of time-varying disturbances. (a) Case 1. (b) Case 2. (c) Case 3.

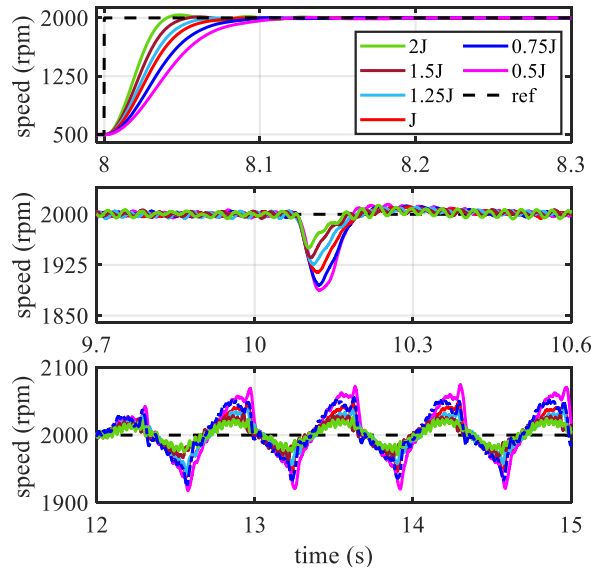


Fig. 16. Speed response curves with the system under different J .

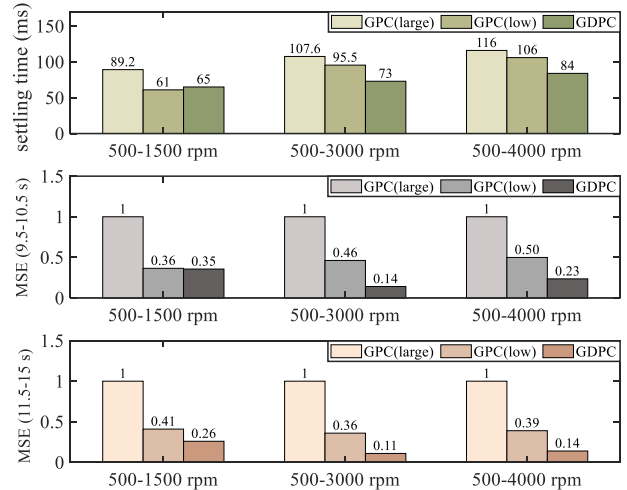


Fig. 17. Performance indices under GPC (large/low) and the GDPC methods.

speed regulation, the proposed GDPC approach effectively improves dynamic performance and endows the system with enhanced disturbance attenuation capability.

TABLE IV
CALCULATED PERFORMANCE INDICES

Index → Method	Case	OS (%)			SD (rpm)			SF (rpm)		
		1	2	3	1	2	3	1	2	3
PI-PI		8.42	6.01	6.21	345	352	93	806	950	187
LADRC		4.20	4.56	0.68	120	116	32	232	252	46
GPC (large)		0.50	0.07	0.06	145	134	22	73	181	35
GPC (low)		0.30	0.08	0.17	99	94	15	56	115	24
GDPC		0.46	0.52	0.04	94	45	9	52	61	15

VII. CONCLUSIONS

In this paper, to alleviate the performance optimization capability limitation of the traditional fixed-horizon-based GPC approaches, a novel composite GDPC synthesis scheme has been proposed for speed regulation of the PMSM drives with a non-cascade structure. The DUEA technique has been em-

ployed to compensate for the matched and time-varying mismatched disturbances estimated by HOSMOs in the receding-horizon optimization, achieving offset-free tracking of the given speed in the presence of disturbances. Furthermore, a novel self-tuning horizon mechanism has been developed to adjust the prediction horizon in real-time according to the operating conditions, enabling dynamic adjustment of performance optimization effects. Comprehensive controller design and stability analysis have also been presented. Finally, comparative simulations and experiments were performed to validate the effectiveness of the proposed methodology. These results demonstrate that the proposed GDPC method provides faster transient performance and enhanced disturbance rejection capability under a wide range of operating conditions while featuring low computational burden compared to MPCs.

APPENDIX

To verify the theoretical soundness of the newly proposed control strategy, its rigorous stability analysis is presented next.

Proof: The whole proof process is divided into the following two cases.

Case 1: Both the current and voltage are not saturated, i.e., $i_q \in [-I_{\max}, I_{\max}]$ and $u_{cq} \in [u_{v_min}, u_{v_max}]$.

In this case, the u_{cq} generated by the proposed controller (16) satisfies $u_{cq}(t) = u_q(t)$. With this in mind, introduce the coordinate transformations $\xi_\omega = \frac{\hat{\delta}_\omega}{l_q}$, $\xi_q = \frac{\hat{\delta}_q}{l_q^{1/2}}$ and $\varsigma_q = \frac{\hat{v}_q}{l_q^{3/2}}$. Combining the system error dynamics (8) with (16), one can obtain the closed-loop system

$$\dot{\xi}_\alpha = l_q(\mathbf{A} - \mathbf{B}\mathbf{K}_\alpha)\xi_\alpha - \frac{i_q}{l_q}\mathbf{M}\xi_\alpha + \mathbf{E} + \mathbf{F}_1, \quad (25)$$

where $\xi_\alpha = [\xi_\omega, \xi_q]^\top$, $\mathbf{K}_\alpha = \begin{bmatrix} k_\omega^*, k_q^* \\ T_0^2, T_0 \end{bmatrix}$, $\mathbf{M} = \text{diag}\{1, 2\}$, $\mathbf{E} = \begin{bmatrix} \zeta_1, \zeta_2 \\ l_q, l_q^{1/2} \end{bmatrix}^\top$, $\mathbf{F}_1 = \begin{bmatrix} \frac{f_1(\bar{\mathbf{x}}) - f_1(\hat{\bar{\mathbf{x}}}^*)}{l_q}, \frac{f_2(\bar{\mathbf{x}}) - f_2(\hat{\bar{\mathbf{x}}}^*)}{l_q^2} \end{bmatrix}^\top$.

On the basis of (25), one can verify that the system matrix $(\mathbf{A} - \mathbf{B}\mathbf{K}_\alpha)$ is always Hurwitz stable. Therefore, one can get

$$(\mathbf{A} - \mathbf{B}\mathbf{K}_\alpha)^\top \mathbf{Q} + \mathbf{Q}(\mathbf{A} - \mathbf{B}\mathbf{K}_\alpha) = -\mathbf{I}_{2 \times 2}, \quad (26)$$

where $\mathbf{Q} = \mathbf{Q}^\top$ is a positive definite matrix.

Next, construct the Lyapunov candidate function as $V(\xi_\alpha) = \xi_\alpha^\top \mathbf{Q} \xi_\alpha$. Then, the following inequality holds

$$\lambda_{\min}(\mathbf{Q})\|\xi_\alpha\|^2 \leq V \leq \lambda_{\max}(\mathbf{Q})\|\xi_\alpha\|^2, \quad (27)$$

where $\lambda_{\max}(\cdot)$ and $\lambda_{\min}(\cdot)$ generally represent the maximum and minimum eigenvalues of the matrix (\cdot) , respectively.

Taking the derivative of V along system (25) yields

$$\begin{aligned} \dot{V} &= -l_q\|\xi_\alpha\|^2 - \frac{i_q}{l_q}\xi_\alpha^\top \mathbf{W}\xi_\alpha + 2\mathbf{F}_1^\top \mathbf{Q}\xi_\alpha + 2\mathbf{E}^\top \mathbf{Q}\xi_\alpha \\ &\leq -l_q\|\xi_\alpha\|^2 + 2\lambda_{\max}(\mathbf{Q})(\|\mathbf{E}\| + \|\mathbf{F}_1\|)\|\xi_\alpha\| \\ &\quad - \frac{i_q}{l_q}\xi_\alpha^\top \mathbf{W}\xi_\alpha, \end{aligned} \quad (28)$$

where $\mathbf{W} = (\mathbf{M}^\top \mathbf{Q} + \mathbf{Q}\mathbf{M})$.

Now, by defining $\kappa_1 = \frac{k_\omega^*}{T_0^2}$ and $\kappa_2 = \frac{k_q^*}{T_0}$, the matrix \mathbf{Q} can be resolved by (26) as $\mathbf{Q} = \frac{1}{2} \cdot \begin{bmatrix} \frac{\kappa_1 + \kappa_1^2 + \kappa_2^2}{\kappa_1 \kappa_2} & \frac{1}{\kappa_1} \\ \frac{1}{\kappa_1} & \frac{1 + \kappa_1}{\kappa_1 \kappa_2} \end{bmatrix}$.

It is easy to prove that \mathbf{W} is positive definite by k_ω^* and k_q^* in (14). Meanwhile, based on the mathematical scaling method in [41], with $l_q \geq 1$ in mind, one can obtain that

$$\begin{aligned} \frac{f_1(\bar{\mathbf{x}}) - f_1(\hat{\bar{\mathbf{x}}}^*)}{l_q} &\leq c_1 \left(\frac{|x_1 - \hat{x}_1^*|}{l_q} \right) \leq c_1(|\xi_\omega| + |\xi_q|), \\ \frac{f_2(\bar{\mathbf{x}}) - f_2(\hat{\bar{\mathbf{x}}}^*)}{l_q^2} &\leq c_2 \left(\frac{|x_1 - \hat{x}_1^*|}{l_q} + \frac{|x_2 - \hat{x}_2^*|}{l_q^2} \right) \\ &\leq c_2(|\xi_\omega| + |\xi_q|), \end{aligned} \quad (29)$$

where c_1 and c_2 are positive constants.

Then, with (29) in mind, inequality (28) can be reduced to

$$\dot{V} \leq -(l_q - \iota)\|\xi_\alpha\|^2 + 2\lambda_{\max}(\mathbf{Q})\|\mathbf{E}\|\|\xi_\alpha\|, \quad (30)$$

where $\iota = \lambda_{\max}(\mathbf{Q})(4\tilde{c}^2 + 1)$ and $\tilde{c} = \max\{c_1, c_2\}$.

It is demonstrated from Th.5 in [31] that for system (2), under *Assumption 1*, if the gains λ_i in (5) and (6) are suitably chosen and satisfy $\lambda_i \geq D$, $i = 1, 2$, then there exists a finite-time constant t_1 and a bounded constant \mathcal{E} , such that $\zeta_i(t) \equiv 0$ when $t \in [t_1, \infty)$ and $\sup\{|\zeta_i(t)|\} \leq \mathcal{E}$ when $t \in [0, t_1]$. Therefore, (30) can be further reformulated as

$$\dot{V} \leq -(l_q - \sigma_1)\|\xi_\alpha\|^2 + \mathcal{E}^2, \quad (31)$$

where $\sigma_1 = 2\lambda_{\max}^2(\mathbf{Q}) + \iota$.

Further analysis is conducted in the following three steps:

1) *Boundedness of the Self-Tuning Horizon:* With (15) in mind, it is evident that if l_q is bounded, then T_1 must also be bounded. One can make a hypothesis that l_q will diverge to infinity in finite time t_f , i.e., $\lim_{t \rightarrow t_f} l_q(t) = \infty$. Under the premise that this hypothesis is established, it is obvious that there always exists a finite-time constant $t^* \in [0, t_f)$ satisfying $l_q(t^*) \geq \sigma_1 + 1$. Then, with (15) and (31) in mind, the following statement holds

$$\begin{aligned} \int_{t^*}^{t_f} l_q(t) d\tau &\leq 2\rho \int_{t^*}^{t_f} \|\xi_\alpha\|^2 d\tau \leq 2\rho \int_{t^*}^{t_f} \mathcal{E}^2 - \dot{V}(t) d\tau \\ &= 2\rho [V(t^*) - V(t_f) + \mathcal{E}^2(t_f - t^*)] = \text{constant}. \end{aligned} \quad (32)$$

It is apparent that the expression (32) contradicts the assumption above, thus one can conclude that the adaptive bandwidth factor l_q has an upper bound, i.e., there is a lower bound for the horizon T_1 .

2) *Boundedness of the System States:* Considering the time interval $t \in [0, t_2)$, where $t_2 = \max\{t_1, t^*\}$, (31) can be further estimated by

$$\dot{V} \leq K_v V + L_v \quad (33)$$

where $K_v = \frac{|l_q - \sigma_1|}{\lambda_{\min}(\mathbf{Q})}$ and $L_v = \mathcal{E}^2$. It follows from (33) that the solution of V satisfies $V \leq -\frac{L_v}{K_v} + (V(0) + \frac{L_v}{K_v})e^{K_v t}$. This indicates that the system states are bounded in the considered time interval $t \in [0, t_2)$.

3) *Asymptotic Convergence of the System Outputs:* When $t \in [t_2, +\infty)$, with the conditions $\zeta_i(t) = 0$, $l_q(t^*) \geq \sigma_1 + 1$ in mind, (31) can be further reduced to

$$\dot{V} \leq -\Gamma_v V \quad (34)$$

where $\Gamma_v = \frac{(l_q - \sigma_1)}{\lambda_{\max}(\mathbf{Q})}$. Inequality (34) reveals that the states of system (9) will asymptotically converge to 0.

Case 2: The current or voltage is saturated, i.e., $u_{cq} \notin [u_{min}, u_{max}]$.

Note that the analysis presented above is based on the case where (23) is not activated. However, under certain extreme operating conditions, such as encountering a wide step speed switching or heavy loads, (23) may be triggered intermittently during transient phases. In such instance, u_{cq} will be modified to ensure safety. It can be caused by the following basic cases.

The first case is when the current limitation (17) is triggered, i.e., $u_{cq} \notin [u_{i_min}, u_{i_max}]$. In this situation, the voltage boundary value of either u_{i_min} or u_{i_max} is enforced on u_q . The second scenario occurs when voltage limitation (22) is triggered, i.e., $u_{cq} \notin [u_{v_min}, u_{v_max}]$. In this case, the u_q is forced to the voltage boundary value u_{v_min} or u_{v_max} . However, in either case, the control input u_1 is bounded by $|u_1| \leq Z$, where $Z \geq \frac{3n_p\psi_f}{2JL_s} \max\{|\bar{u}_{min}|, |\bar{u}_{max}|\}$ is a positive constant, with $\bar{u}_{max} = \max\{u_{max}(n)\}$ and $\bar{u}_{min} = \min\{u_{min}(n)\}$, $n \in \{0, 1, 2, 3, \dots, \infty\}$.

Assuming that d -axis current controller works well, i.e., $i_d = 0$, the system (2) can be reformulated as

$$\dot{\bar{x}} = \mathbf{A}_s \bar{x} + \mathbf{U}, \quad (35)$$

where $\mathbf{A}_s = \begin{bmatrix} -a_1 & 1 \\ -a_2 & -a_3 \end{bmatrix}$, $\mathbf{U} = \begin{bmatrix} d_1 \\ u_1 + C_1 + d_2 \end{bmatrix}$, $a_1 = \frac{B_m}{J}$, $a_2 = \frac{3n_p^2\psi_f^2}{2JL_s}$ and $a_3 = \frac{R_s}{L_s}$.

It is easy to verify that \mathbf{A}_s is Hurwitz stable. Therefore, there exists a symmetric positive definite matrix \mathbf{Q}_s such that

$$\mathbf{A}_s^\top \mathbf{Q}_s + \mathbf{Q}_s \mathbf{A}_s = -\mathbf{I}_{2 \times 2}. \quad (36)$$

Define a candidate Lyapunov function as $V_u = \bar{x}^\top \mathbf{Q}_s \bar{x}$, and take the derivative of V_u along system dynamics (35) yields

$$\begin{aligned} \dot{V}_u &= -\|\bar{x}\|^2 + 2\mathbf{U}^\top \mathbf{Q}_s \bar{x} \leq -\|\bar{x}\|^2 + 2\lambda_{\max}(\mathbf{Q}_s) \|\mathbf{U}\| \|\bar{x}\| \\ &\leq -(1 - \frac{1}{2}) \|\bar{x}\|^2 + 2\lambda_{\max}^2(\mathbf{Q}_s) \|\mathbf{U}\|^2 \\ &\leq -\Gamma_u V_u + \Delta, \end{aligned} \quad (37)$$

where $\Gamma_u = \frac{1}{2\lambda_{\max}(\mathbf{Q}_s)}$, $\Delta = 2\lambda_{\max}^2(\mathbf{Q}_s) L_u^2$, and $L_u = D + Z + C_1$.

Similar to (33), it is easy to obtain from (37) that

$$V_u \leq \frac{\Delta}{\Gamma_u} + (V_u(0) - \frac{\Delta}{\Gamma_u}) e^{-\Gamma_u t}. \quad (38)$$

Inequality (38) proves that V_u is bounded, thus the system states in (2) are also bounded.

The proof of Theorem 1 is thus completed. ■

REFERENCES

- [1] Z. Hao, Y. Yang, Y. Gong, Z. Hao, C. Zhang, H. Song, and J. Zhang, "Linear/nonlinear active disturbance rejection switching control for permanent magnet synchronous motors," *IEEE Transactions on Power Electronics*, vol. 36, no. 8, pp. 9334–9347, 2021.
- [2] F. Wang, L. He, and J. Rodriguez, "FPGA-based continuous control set model predictive current control for PMSM system using multistep error tracking technique," *IEEE Transactions on Power Electronics*, vol. 35, no. 12, pp. 13 455–13 464, 2020.
- [3] D.-W. Seo, Y. Bak, and K.-B. Lee, "An improved rotating restart method for a sensorless permanent magnet synchronous motor drive system using repetitive zero voltage vectors," *IEEE Transactions on Industrial Electronics*, vol. 67, no. 5, pp. 3496–3504, 2019.
- [4] J. Liu, C. Gong, Z. Han, and H. Yu, "IPMSM model predictive control in flux-weakening operation using an improved algorithm," *IEEE Transactions on Industrial Electronics*, vol. 65, no. 12, pp. 9378–9387, 2018.
- [5] N. Bedetti, S. Calligaro, and R. Petrella, "Analytical design and auto-tuning of adaptive flux-weakening voltage regulation loop in IPMSM drives with accurate torque regulation," *IEEE Transactions on Industry Applications*, vol. 56, no. 1, pp. 301–313, 2020.
- [6] J. Lara, J. Xu, and A. Chandra, "Effects of rotor position error in the performance of field-oriented-controlled PMSM drives for electric vehicle traction applications," *IEEE Transactions on Industrial Electronics*, vol. 63, no. 8, pp. 4738–4751, 2016.
- [7] H. Kawai, Z. Zhang, R. Kennel, and S. Dokic, "Direct speed control based on finite control set model predictive control with voltage smoother," *IEEE Transactions on Industrial Electronics*, vol. 70, no. 3, pp. 2363–2372, 2022.
- [8] S. Ding, Q. Hou, and H. Wang, "Disturbance-observer-based second-order sliding mode controller for speed control of PMSM drives," *IEEE Transactions on Energy Conversion*, vol. 38, no. 1, pp. 100–110, 2023.
- [9] Q. Hou, S. Ding, and X. Yu, "Composite super-twisting sliding mode control design for PMSM speed regulation problem based on a novel disturbance observer," *IEEE Transactions on Energy Conversion*, vol. 36, no. 4, pp. 2591–2599, 2021.
- [10] D. M. Garduño, J. J. Rivas, O. C. Castillo, R. O. González, and F. E. R. Gutiérrez, "Current distortion rejection in PMSM drives using an adaptive super-twisting algorithm," *IEEE Transactions on Energy Conversion*, vol. 37, no. 2, pp. 927–934, 2022.
- [11] Z. Li, F. Wang, D. Ke, J. Li, and W. Zhang, "Robust continuous model predictive speed and current control for PMSM with adaptive integral sliding-mode approach," *IEEE Transactions on Power Electronics*, vol. 36, no. 12, pp. 14 398–14 408, 2021.
- [12] Y. Zuo, J. Mei, C. Jiang, X. Yuan, S. Xie, and C. H. Lee, "Linear active disturbance rejection controllers for PMSM speed regulation system considering the speed filter," *IEEE Transactions on Power Electronics*, vol. 36, no. 12, pp. 14 579–14 592, 2021.
- [13] J. Yang, W.-H. Chen, S. Li, L. Guo, and Y. Yan, "Disturbance/uncertainty estimation and attenuation techniques in PMSM drives—A survey," *IEEE Transactions on Industrial Electronics*, vol. 64, no. 4, pp. 3273–3285, 2017.
- [14] R. Zhou, C. Fu, and W. Tan, "Implementation of linear controllers via active disturbance rejection control structure," *IEEE Transactions on Industrial Electronics*, vol. 68, no. 7, pp. 6217–6226, 2020.
- [15] Y. Yan, X.-F. Wang, B. J. Marshall, C. Liu, J. Yang, and W.-H. Chen, "Surviving disturbances: A predictive control framework with guaranteed safety," *Automatica*, vol. 158, p. 111238, 2023.
- [16] C. Garcia, J. Rodriguez, C. Silva, C. Rojas, P. Zanchetta, and H. Abu-Rub, "Full predictive cascaded speed and current control of an induction machine," *IEEE Transactions on Energy Conversion*, vol. 31, no. 3, pp. 1059–1067, 2016.
- [17] X. Li, W. Tian, X. Gao, Q. Yang, and R. Kennel, "A generalized observer-based robust predictive current control strategy for PMSM drive system," *IEEE Transactions on Industrial Electronics*, vol. 69, no. 2, pp. 1322–1332, 2021.
- [18] W. Tu, G. Luo, Z. Chen, L. Cui, and R. Kennel, "Predictive cascaded speed and current control for PMSM drives with multi-timescale optimization," *IEEE Transactions on Power Electronics*, vol. 34, no. 11, pp. 11 046–11 061, 2019.
- [19] M. Zhou, X. Liu, and S. Li, "Composite single-loop model predictive control design for PMSM servo system speed regulation based on disturbance observer," in 2020 Chinese Control and Decision Conference (CCDC), Hefei, China, 2020, pp. 2886–2892.
- [20] K. Belda and D. Vošmík, "Explicit generalized predictive control of speed and position of PMSM drives," *IEEE Transactions on Industrial Electronics*, vol. 63, no. 6, pp. 3889–3896, 2016.
- [21] X. Gao, M. Abdelrahem, C. M. Hackl, Z. Zhang, and R. Kennel, "Direct predictive speed control with a sliding manifold term for PMSM drives," *IEEE Journal of Emerging and Selected Topics in Power Electronics*, vol. 8, no. 2, pp. 1258–1267, 2020.
- [22] J. Mao, H. Li, L. Yang, H. Zhang, L. Liu, X. Wang, and J. Tao, "Non-cascaded model-free predictive speed control of SMPMSM drive system," *IEEE Transactions on Energy Conversion*, vol. 37, no. 1, pp. 153–162, 2022.
- [23] M. Preindl and S. Bolognani, "Model predictive direct speed control with finite control set of PMSM drive systems," *IEEE Transactions on Power Electronics*, vol. 28, no. 2, pp. 1007–1015, 2012.
- [24] M. Liu, K. W. Chan, J. Hu, W. Xu, and J. Rodriguez, "Model predictive direct speed control with torque oscillation reduction for PMSM drives,"

- [24] *IEEE Transactions on Industrial Informatics*, vol. 15, no. 9, pp. 4944–4956, 2019.
- [25] J. Liu, J. Yang, S. Li, and X. Wang, “Single-loop robust model predictive speed regulation of PMSM based on exogenous signal preview,” *IEEE Transactions on Industrial Electronics*, vol. 70, no. 12, pp. 12 719–12 729, 2023.
- [26] C. Dai, T. Guo, J. Yang, and S. Li, “A disturbance observer-based current-constrained controller for speed regulation of PMSM systems subject to unmatched disturbances,” *IEEE Transactions on Industrial Electronics*, vol. 68, no. 1, pp. 767–775, 2020.
- [27] J. Yang, W. X. Zheng, S. Li, B. Wu, and M. Cheng, “Design of a prediction-accuracy-enhanced continuous-time MPC for disturbed systems via a disturbance observer,” *IEEE Transactions on Industrial Electronics*, vol. 62, no. 9, pp. 5807–5816, 2015.
- [28] X. Dong, J. Mao, Y. Yan, C. Zhang, and J. Yang, “Generalized dynamic predictive control for nonlinear systems subject to mismatched disturbances with application to PMSM drives,” *IEEE Transactions on Industrial Electronics*, vol. 71, no. 1, pp. 954–964, 2024.
- [29] C. Zhang, M. Li, L. Zhou, C. Cui, and L. Xu, “A variable self-tuning horizon mechanism for generalized dynamic predictive control on DC/DC boost converters feeding CPLs,” *IEEE Journal of Emerging and Selected Topics in Power Electronics*, vol. 11, no. 2, pp. 1650–1660, 2022.
- [30] Y. Yan, C. Zhang, A. Narayan, J. Yang, S. Li, and H. Yu, “Generalized dynamic predictive control for nonparametric uncertain systems with application to series elastic actuators,” *IEEE Transactions on Industrial Informatics*, vol. 14, no. 11, pp. 4829–4840, 2018.
- [31] A. Levant, “Higher-order sliding modes, differentiation and output-feedback control,” *International Journal of Control*, vol. 76, no. 9, pp. 924–941, 2003.
- [32] T. Tarczewski and L. M. Grzesiak, “Constrained state feedback speed control of PMSM based on model predictive approach,” *IEEE Transactions on Industrial Electronics*, vol. 63, no. 6, pp. 3867–3875, 2016.
- [33] P. Cortes, M. P. Kazmierkowski, R. M. Kennel, D. E. Quevedo, and J. Rodriguez, “Predictive control in power electronics and drives,” *IEEE Transactions on Industrial Electronics*, vol. 55, no. 12, pp. 4312–4324, 2008.
- [34] Z. Yang, C. Miao, and X. Sun, “Model predictive current control for IPMSM drives with extended-state-observer-based sliding mode speed controller,” *IEEE Transactions on Energy Conversion*, vol. 38, no. 2, pp. 1471–1480, 2023.
- [35] A. Khlaief, M. Bendjedia, M. Boussak, and M. Gossa, “A nonlinear observer for high-performance sensorless speed control of IPMSM drive,” *IEEE Transactions on Power Electronics*, vol. 27, no. 6, pp. 3028–3040, 2012.
- [36] Q. Tang, A. Shen, P. Luo, H. Shen, W. Li, and X. He, “IPMSMs sensorless MTPA control based on virtual q-axis inductance by using virtual high-frequency signal injection,” *IEEE Transactions on Industrial Electronics*, vol. 67, no. 1, pp. 136–146, 2020.
- [37] C.-T. Pan and S.-M. Sue, “A linear maximum torque per ampere control for IPMSM drives over full-speed range,” *IEEE Transactions on Energy Conversion*, vol. 20, no. 2, pp. 359–366, 2005.
- [38] S. Morimoto, M. Sanada, and Y. Takeda, “Wide-speed operation of interior permanent magnet synchronous motors with high-performance current regulator,” *IEEE Transactions on Industry Applications*, vol. 30, no. 4, pp. 920–926, 1994.
- [39] Z. Tang, X. Li, S. Dusmez, and B. Akin, “A new V/f-based sensorless MTPA control for IPMSM drives,” *IEEE Transactions on Power Electronics*, vol. 31, no. 6, pp. 4400–4415, 2016.
- [40] W. Xu, M. M. Ismail, Y. Liu, and M. R. Islam, “Parameter optimization of adaptive flux-weakening strategy for permanent-magnet synchronous motor drives based on particle swarm algorithm,” *IEEE Transactions on Power Electronics*, vol. 34, no. 12, pp. 12 128–12 140, 2019.
- [41] C. Zhang, J. Yang, Y. Yan, L. Fridman, and S. Li, “Semiglobal finite-time trajectory tracking realization for disturbed nonlinear systems via higher-order sliding modes,” *IEEE Transactions on Automatic Control*, vol. 65, no. 5, pp. 2185–2191, 2020.



Zhongkun Cao (Student Member, IEEE) received the B.Sc. degree in Automation from Linyi University in 2021. He is currently pursuing the M.Sc. degree with the College of Automation Engineering, Shanghai University of Electric Power, China, and under the guidance of Prof. C. Zhang and Dr. J. Mao. He is a member of Intelligent Autonomous Systems (IAS) Laboratory.

His research interests include model predictive control of permanent magnet synchronous motors.



Jianliang Mao (Member, IEEE) received the B.Sc. degree in automation, the M.Sc. degree in control engineering, and the Ph.D. degree in control theory and control engineering from the School of Automation, Southeast University, Nanjing, China, in 2011, 2014, and 2018, respectively.

From 2018 to 2021, he worked at the Research and Development Institute, Estun Automation Co., Ltd, Nanjing, China. Since 2021, he joined the College of Automation Engineering, Shanghai University of Electric Power. His research interests include

model predictive control, sliding mode control, vision-based interactive control and their applications to electric drives and robot manipulators.



Xin Dong (Member, IEEE) received the B.Sc. and M.Sc., degrees in electrical engineering from Southeast University and Chengxian College and the College of Automation Engineering, Shanghai University of Electric Power, in 2019 and 2022, respectively.

He is with the College of Automation Engineering, Shanghai University of Electric Power. He is a member of Intelligent Autonomous Systems Laboratory. His research interests include nonlinear control theory and applications for electric power system.



Rafal Madonski (Senior Member, IEEE) received the B.Eng, M.Sc., and Ph.D. degrees in automation and robotics from the Poznan University of Technology, Poland, in 2009, 2010, and 2016, respectively.

He was a Postdoc Researcher with the School of Automation, Southeast University, Nanjing, China, from 2017 to 2019. In 2020, he joined the Energy and Electricity Research Center, Jinan University, Zhuhai, China as an Associate Professor. Recently, he was with the Faculty of Automatic Control, Electronics and Computer Science, Silesian University of Technology, Gliwice, Poland. His research interests are design, analysis, and application of active disturbance rejection control (ADRC).



Chuanlin Zhang (Senior Member, IEEE) received the B.S. degree in mathematics and the Ph.D. degree in control theory and control engineering from the School of Automation, Southeast University, Nanjing, China, in 2008 and 2014, respectively.

He was a Visiting Ph.D. Student with the Department of Electrical and Computer Engineering, University of Texas at San Antonio, USA, from 2011 to 2012; a Visiting Scholar with the Energy Research Institute, Nanyang Technological University, Singapore, from 2016 to 2017. Since 2014, he has been

with the College of Automation Engineering, Shanghai University of Electric Power, Shanghai, where he is currently a Professor. His research interests include nonlinear system control theory and applications for power systems.



Jun Yang (Fellow, IEEE) received the B.Sc. degree in automation from the Department of Automatic Control, Northeastern University, Shenyang, China, and the Ph.D. degree in control theory and control engineering from the School of Automation, Southeast University, Nanjing, China, in 2006 and 2011, respectively. Since 2020, he has been with the Department of Aeronautical and Automotive Engineering, Loughborough University, Loughborough, U.K., as a Senior Lecturer. His research interests include disturbance observer, motion control, visual servoing, nonlinear control, and autonomous systems.

Dr. Yang was the recipient of the EPSRC New Investigator Award. He serves as Associate Editor or Technical Editor for IEEE Transactions on Industrial Electronics, IEEE-ASME Transactions ON Mechatronics, IEEE Open Journal of Industrial Electronics Society, etc. He is a Fellow of IET.